Journal of Drug Delivery Science and Technology 116 (2026) 107937

Contents lists available at ScienceDirect

Journal of Drug Delivery Science and Technology

journal homepage: www.elsevier.com/locate/jddst

Research paper

Caffeic acid–functionalized silver nanoparticles for skin therapy: Antioxidant, antibacterial, and anti-melanogenic properties

Siham Bouaouz [a], Rebeca Lozano [a], Francisca I. Bravo [c,d,e], Begoña Muguerza [c,d,e], Miquel Mulero [c,d,e], Enrique Calvo [c,d,e,*], Paula Ortega [a,b,**], F. Javier de la Mata [a,b,***]

[a] Universidad de Alcalá. Department of Organic and Inorganic Chemistry, Research Institute in Chemistry "Andrés M. del Río" (IQAR), Madrid, Spain
[b] Networking Research Center on Bioengineering, Biomaterials and Nanomedicine (CIBER-BBN), Spain and Institute "Ramón y Cajal" for Health Research (IRYCIS), Spain
[c] Nutrigenomics Research Group, Department of Biochemistry and Biotechnology, Universitat Rovira i Virgili, Tarragona, Spain
[d] Institute of Health Research Pere Virgili (IISPV), Tarragona, Spain
[e] Center of Environmental, Food and, Toxicological Technology (TecnATox), University Rovira i Virgili, Tarragona, Spain

ARTICLE INFO

Keywords:
Silver nanoparticles
Caffeic acid
Melanogenic activity
Antioxidant
Antibacterial

ABSTRACT

Multifunctional nanomaterials offers promising strategies for the treatment of skin disorders involving oxidative stress, microbial infections, and hyperpigmentation. Herein, we report the covalent functionalization of silver nanoparticles AgNP-(S-PEG2K-CA) (AgNP-1) with caffeic acid, a natural polyphenol with well-known antioxidant and anti-melanogenic properties. Additionally, a cationic carbosilane wedge was introduced to confer antibacterial functionality, resulting in a heterofunctional nanoconjugate, AgNP-(S-PEG2K-CA)(S-G_1-NMe_3Cl) (AgNP-2), with enhanced biological performance. The physicochemical characterization confirmed successful functionalization and stability of the nanoparticles. Biological assays showed that the silver nanoparticles exhibited antioxidant activity (AgNP-1: IC_{50} = 4.18 μg/mL, EC_{50} = 0.57 μg/mL; AgNP-2: IC_{50} = 12.35 μg/mL, EC_{50} = 0.87 μg/mL), which was attributed to the presence of caffeic acid on their surface and AgNP-2 exhibited strong antibacterial effects, particularly against *Staphylococcus aureus* (MIC 4 mgL^{-1} and MBC 8 mgL^{-1}) and *Escherichia coli* (MIC 4 mgL^{-1} and MBC 8 mgL^{-1}). In vitro experiments using a mammalian melanocyte model (B16F10 cells) revealed for both nanoparticles significantly inhibited melanin synthesis at 20 μg/mL reduced the accumulation of intracellular melanin in a similar extent as kojic acid at 1000 μg/mL. Finally, permeation studies using Franz diffusion cells, combined with UV–Vis spectroscopy and ICP-OES analysis to detect nanoparticle concentration, showed that neither AgNP-1 nor AgNP-2 were able to cross the membrane, indicating that they remain confined to the membrane surface. This localization is crucial for minimizing the risk of systemic exposure, thereby supporting the safety and suitability of these nanoparticles for topical applications.

1. Introduction

Melanogenesis, the biological process responsible for the synthesis of melanin, the pigment that determines skin, hair, and eye colour in humans and other organisms, represents a critical area of study in cellular biology and dermatology [1]. Within this context, the enzyme tyrosinase emerges as a central figure in the metabolic cascade leading to melanin formation.

The molecular and cellular mechanisms regulating tyrosinase activity play a substantial role in pathological conditions associated with hyperpigmentation, such as melasma, freckles, and other pigmentary disorders, garnering intense attention [2]. Numerous published studies have investigated the inhibition of tyrosinase as a promising therapeutic approach for treating skin diseases related to hyperpigmentation [3,4].

* Corresponding author. Nutrigenomics Research Group, Department of Biochemistry and Biotechnology, Universitat Rovira i Virgili, Tarragona, Spain.
** Corresponding author. Universidad de Alcalá. Department of Organic and Inorganic Chemistry, Research Institute in Chemistry "Andrés M. del Río" (IQAR), Madrid, Spain.
*** Corresponding author. Universidad de Alcalá. Department of Organic and Inorganic Chemistry, Research Institute in Chemistry "Andrés M. del Río" (IQAR), Madrid, Spain.
E-mail addresses: enrique.calvo@urv.cat (E. Calvo), paula.ortega@uah.es (P. Ortega), javier.delamata@uah.es (F.J. de la Mata).

https://doi.org/10.1016/j.jddst.2025.107937
Received 6 September 2025; Received in revised form 11 December 2025; Accepted 16 December 2025
Available online 16 December 2025

A wide range of tyrosinase inhibitors has been explored [3,5,6]. Among these, polyphenolic compounds stand out due to their multifaceted biological effects. In addition to their capacity to modulate tyrosinase activity, thus regulating melanin production, polyphenols exhibit noteworthy antioxidant and anti-inflammatory properties, making them particularly attractive candidates for therapeutic intervention [7–9]. However, many polyphenols exhibit low water solubility, low bioavailability and rapid elimination via excretion renal or fecal excretion limiting their exposure time to target tissues. Consequently, their therapeutic efficacy is compromised, often necessitating high drug doses and frequent administration. To mitigate these challenges and enhance polyphenol biodistribution, diverse strategies are under investigation. These include encapsulation within controlled-release systems, chemical derivatization to enhance solubility and stability, synergistic formulations with other bioactive compounds, and optimization of natural product formulation and delivery methods [10–13].

Metallic nanoparticles are valuable therapeutic agents in the field of dermatology and cosmetics offering a wide range of applications in skin treatment, from sun protection and wound healing to photothermal therapy, drug delivery, and dermatological diagnostics [14–16]. To date, numerous studies have focused on the green synthesis of metal nanoparticles decorated with polyphenols to combine the unique biological properties of both systems. This approach leverages the ability of the hydroxyl groups of polyphenols to reduce the metal center, facilitating the formation of metal-polyphenol nanomaterials (MPNs) [17–20]. The *in vitro* inhibition of mushroom tyrosinase enzyme by various silver nanoparticles (AgNPs) synthesized through biogenic methods using microorganisms and/or plant extracts has been demonstrated. Although the mechanism of enzyme inhibition remains unclear, one hypothesis relates to the nature of its active centre, which consists of two copper atoms, each coordinated to three histidine residues. This suggests that AgNPs might inhibit the enzyme by replacing the copper ion with silver, since copper homeostasis is involved in the activation of the pigmentation-causing enzyme [21–24]. Regarding polyphenolic compounds, they exert their inhibitory effect on tyrosinase through various mechanisms, including chelation of copper ions at the enzyme's active site, modulation of gene expression related to melanogenesis, and inhibition the enzymatic conversion of dopaquinone to melanin within melanocytes. These actions prevent the accumulation of melanin pigments in the skin, leading to a lightning effect [25,26]. An alternative hypothesis proposes that the compound attenuates melanogenesis by suppressing the mitogen-activated protein kinase (MAPK) cascade (specifically the ERK, JNK, and p38 branches), thereby blocking the sequential activation of downstream transcriptional regulators. In normal melanocytes, phosphorylation of ERK, JNK, and p38 enhances the phosphorylation of CREB, which then binds to cAMP response elements within the promoter of the microphthalmia-associated transcription factor (MITF) gene, thereby driving its transcription. MITF upregulates a battery of melanogenic enzymes, foremost the tyrosinase gene (TYR), whose product is essential for the first and rate-limiting steps of melanin synthesis. In this context, reactive oxygen species (ROS) act as chemical messengers that activate intracellular signalling pathways, including the MAPK cascade [27]. Compounds functionalized with polyphenols have demonstrated to exert antioxidant properties, effectively reducing intracellular ROS levels. By lowering ROS availability, these polyphenol-functionalized nanoparticles may attenuate ROS-mediated activation of the MAPK pathway, thereby reducing CREB phosphorylation, downregulating MITF expression, and ultimately suppressing tyrosinase transcription and melanin production. This provides a plausible mechanistic basis for their observed anti-melanogenic activity [28,29].

This study focuses on the synthesis of silver nanoparticles coated with polyethylene glycol (PEG) chains derivatized with caffeic acid (CA), and their evaluation as depigmenting agents. Caffeic acid was selected for nanoparticle functionalization due to its high natural abundance, versatile chemistry, and well-documented biological relevance. It is one of the most widespread hydroxycinnamic acids in plants and in foods such as coffee, fruits, and wine [30]. Structurally, its catechol and carboxylic groups provide multiple coordination sites for metal binding while retaining strong radical-scavenging activity. In addition, our group has previously employed caffeic acid to obtain stable gold nanoparticles [31] and different carbosilane dendrimers [32], supporting its selection as an optimal polyphenolic modifier for generating robust, bioactive, and biocompatible nanomaterials. Biologically, caffeic acid exhibits potent antioxidant, anti-inflammatory, antimicrobial, and anticancer activities, often associated with modulation of oxidative stress [33]. Beyond its antioxidant role, caffeic acid is also a well-known component of plant extracts traditionally used in skin care due to its effects on inflammation and melanogenesis [34,35]. From a mechanistic perspective, caffeic acid exerts its inhibitory effect by chelating copper ions, which serve as essential cofactors for tyrosinase activity. This chelation disrupts the enzyme-catalyzed oxidation of L-tyrosine to L-DOPA and its subsequent conversion to dopaquinone, representing the initial and rate-limiting steps in the melanin biosynthetic pathway [36]. PEGylation confers a biocompatible surface, minimizing potential cytotoxicity concerns and maximizing compatibility with the delicate skin ecosystem. Also, leveraging the well-established antibacterial properties of silver and the emerging demand for multifunctional solutions in skincare, a novel approach has been developed. Heterofunctional polyphenol-AgNP have been prepared by the integration of a cationic carbosilane dendritic wedges, known for their remarkable antibacterial properties within aqueous media [37,38], onto the surface area. To comprehensively assess the potential application of these novel polyphenol-AgNPs in skincare, we investigated their antioxidant and antibacterial activities against both Gram-positive and Gram-negative bacteria.

2. Materials and methods

2.1. Materials

Silver nitrate ($AgNO_3$), Sodium tetrahydridoborate, ($NaBH_4$), 1-Hydroxybenzotriazole hydrate (HOBt), 2-(dimethylamino)ethanethiol hydrochloride triethylamine (TEA), and HS-PEG2K-NH_2·HCl all purchased from Sigma-Aldrich (UK). 3,4-Dihydroxybenzeneacrylic acid (caffeic acid) purchased from Thermo Fisher Scientific. 1-ethyl-3-(3-dimethylaminopropyl)carbodiimide hydrochloride (EDCI) purchased from Flurochem.

2.2. Methods

All reactions were conducted under an inert atmosphere, with solvents procured and handled under anhydrous conditions. Compounds HS-PEG2K-CA (**I**) [31], HSG_1-NMe_3Cl (**II**) were synthesized as previously reported [39].

Compound HS-PEG2K-CA (I) was obtained by coupling activated caffeic acid (CA) using 1-ethyl-3-(3-dimethylaminopropyl)carbodiimide hydrochloride (EDCI) and 1-hydroxybenzotriazole (HOBt) in N,N-dimethylformamide (DMF) with a thiol-terminated polyethylene glycol amine (HS-PEG2K-NH_2·HCl) in presence of triethylamine (TEA), followed by overnight stirring at 60 °C and purification by dialysis membrane Pre-treated RC Tubing (MWCO: 2 kDa).

Compound HSG_1-NMe_3Cl (II) Compound HSG_1-NMe_3Cl (II) was prepared from BrG_1V2, a first-generation carbosilane scaffold featuring a bromine atom at the focal position and peripheral vinyl moieties, following a synthetic protocol previously established in our laboratory. The terminal vinyl groups underwent a thiolene conjugation with 2-(dimethylamino)ethanethiol hydrochloride ($HSNMe_2$·HCl), yielding the intermediate $MeCOSG_1(SNMe_2·HCl)_2$. This species was subsequently transformed through sequential deprotonation, methylation, and ion-exchange operations, all performed under mild conditions in tetrahydrofuran or methanol/ether mixtures, to afford the final quaternized

dendron [39].

2.3. Nanoparticles characterization

NMR spectra were acquired on either a Varian 500 MHz or Bruker Neo Advance 400 MHz spectrometer, employing Methanol-d_4 (CD_3OD) as the solvent. Chemical shifts (δ) are reported in parts per million (ppm). Assignments of resonance signals were achieved through HSQC, HMBC, and COSY NMR experiments. **Elemental analyses** were carried out using an INTEC EA31OO instrument. **UV–visible** absorption spectra were recorded for homofunctionalized silver nanoparticle samples over a concentration range of 0.071–0.568 mg/mL, and for heterofunctionalized samples ranging from 0.428 to 2.8 mg/mL, to construct calibration curves. All measurements were performed in quartz cuvettes with a 1 cm path length using a PerkinElmer Lambda 18 UV–Vis spectrophotometer. **Transmission electron microscopy (TEM)**: A Carbon-coated copper grid (400 mesh. Sigma-Aldrich) covered with a drop of a 1 mg/mL solution of compounds was dried. Afterward, TEM images were recorded using a transmission electron microscope JEM 2100HT. Image J program was used to measure nanoparticle sizes. **Thermogravimetric analysis (TGA)** Thermal analyses were performed using a TA TGA55 (TA Instruments) on pure, dry samples (2–10 mg). The sample was loaded in a platinum sample holder under nitrogen atmosphere and thermally analyzed under nitrogen from 25 to 1000 °C (10 °C per minute). **Zeta Potential (ZP):** Zeta potential measurements were conducted using a Zetasizer Nano ZS instrument (Malvern Instruments Ltd., UK). Solutions of the compounds (1 mg/mL in deionized water) were passed through a 0.22 μm syringe filter before measurement in disposable Malvern plastic cuvettes. **Dynamic light scattering (DLS):** Hydrodynamic diameter measurements of filtered compound solutions in deionized water (1 mg/mL) were conducted using a Malvern Zetasizer Nano ZS instrument equipped with Non-Invasive Backscatter optics (NBS). The experiments were performed at 25 °C after a prior equilibration period (typically 5 min), and the results were reported as the mean of at least three measurements per sample. **Inductively Coupled Plasma-Optical Emission Spectroscopy (ICP-OES)** was employed to determine the concentration of silver present in the synthesized AgNPs using an ICP-OES Varian 720-ES instrument (Varian Inc., USA). Samples of each compound were measured in triplicate, and results are expressed as the mean ± standard deviation. For silver determination, the calibration curve was prepared by diluting 1:100 from a certified silver standard solution (1000 mg/L, Scharlau, PL00080) in 5 % (v/v) trace metal grade nitric acid (HNO_3, Scharlau) to obtain a stock solution of 10 mg/L. From this stock solution, additional standard solutions at 0.50, 1.00, and 2.00 mg/L were prepared. A 2 mg/L yttrium solution was used as an internal standard (Scharlau). Sample digestion was performed using a Milestone Ethos Easy microwave digestion system equipped with an SR-15 rotor. Approximately 0.5 mL of each sample was digested with 6 mL of trace metal grade HNO_3 at 200 °C for 30 min. After cooling, the digested solutions were diluted to 50 mL with ultrapure water. ICP-OES analysis was conducted under the following operating conditions: plasma power 1.3 kW, plasma gas flow rate 15 L/min, auxiliary gas flow rate 1.5 L/min, nebulizer gas flow rate 1.0 L/min, pump speed 12 rpm, reading time 20 s, stability delay 15 s, sampling delay 20 s, and washing time 30 s. The selected analytical wavelengths for silver were 328.068 nm and 338.289 nm. Results were expressed as milligrams of silver per liter of solution (mg/L). The limit of detection (LOD) was 5 μg/L, and the limit of quantification (LOQ) was 10 μg/L.

2.4. Synthesis of nanoparticles

2.4.1. Synthesis of AgNP-(S-PEG2K-CA) (AgNP-1)

To a deoxygenated aqueous solution of $AgNO_3$ (1.56 mL, 0.0469 mmol, 30 mM, 7.96 mg) was added dropwise an aqueous solution of compound **I** (3.75 mL, 0.0469 mmol, 12.5 mM, 100 mg). Afterward, $NaBH_4$ in deoxygenated water (1.17 mL, 0.2343 mmol, 200 mM, 8.87 mg) was added dropwise, and the mixture remained under stirring over 4 h at room temperature. AgNPs were purified by dialysis (MWCO: 20 kDa) yielding **AgNP-1** as a brown solid dispersed in water. The synthesis was carried out by triplicate (86.2 %). Mean diameter of silver core (TEM): 1.0 nm. The results are expressed as mean ± SEM: Zeta Potential (mV): +1.80 ± 3.12. DLS (Z-average diameter, nm): 18.41 ± 5.50.

2.4.2. Synthesis of AgNP-(S-PEG2K-CA)(S-G_1-NMe_3Cl) (AgNP-2)

Deoxygenated aqueous solutions (1.87 mL, 12.5 mM) of a mixture of compounds **I** (50 mg, 0.0234 mmol) and **II** (10.01 mg, 0.0234 mmol) were added dropwise to a deoxygenated water solution of $AgNO_3$ (0.78 mL, 0.0272 mmol, 30 mM, 3.98 mg). Then, a deoxygenated water solution of $NaBH_4$ (0.59 mL, 0.1172 mmol, 200 mM, 4.44 mg) was added dropwise and the reaction mixture was kept 4 h under stirring at room temperature. Purification by dialysis (MWCO: 20 kDa) yielded **AgNP-2** as a brown solid dispersed in water (88.4 %). The synthesis was performed in triplicate. The results are expressed as mean ± SEM: Zeta Potential (mV): +16.90 ± 3.27 DLS (Z-average diameter, nm): 24.07 ± 1.69.

2.5. Antioxidant activity

2.5.1. DPPH radical scavenging activity

The antioxidant capacity was assessed based on the compounds' ability to scavenge the 1,1-Diphenyl-2-picrylhydrazyl (DPPH) radical. 20 μL of the compounds at concentrations ranging from 0 to 12 μg/mL (homofunctionalized) and 0–14 μg/mL (heterofunctionzalized) were dispensed into 96-well plates. Subsequently, 180 μL aliquots of DPPH methanolic solution (111.11 μM) were added. The absorbance was recorded at 530 nm every 5 min up to 30 min, using a microplate reader (EpochTM, BioTek Instruments, Winooski, VT, USA). All assays were carried out in triplicate, with water serving as the control. The reduction in DPPH absorbance was used to determine scavenging activity. IC_{50} (concentration that produces 50 % of antioxidant activity) was calculated.

2.5.2. Ferric reducing antioxidant power assay (FRAP)

This assay is based on the capacity of antioxidant compounds to reduce the ferric tripyridyltriazine (Fe(III)-TPTZ) complex to the ferrous tripyridyltriazine (Fe(II)-TPTZ) at low pH. To carry out this assay, 20 μL of the compounds in water at concentrations ranging from 0 to 2 μg/mL for both types of nanoparticles were placed in 96 well plates. Then, aliquots of 180 μL of FRAP solution mixed of solutions TPTZ (10 mM solution in 40 mM of hydrochloric acid), $FeCl_3$ (20 mM solution in water) and acetate buffer (20 mM in water, pH 3.6) in a 1:1:10 ratio were added. Following this addition, the absorbance at 593 nm was measured using a microplate reader (EpochTM, BioTek Instruments, Winooski, VT, USA). All experiments were conducted in triplicate, with methanol used as a control. Finally, the EC_{50} (the concentration of antioxidant compound that increases FRAP capacity by 50 %) was calculated.

2.6. Antibacterial activity

The assays were conducted at the Chemistry Research Support Centre of the University of Alcala (CAI-UAH Química). The antibacterial activity of dendritic polyphenols was evaluated *in vitro* against two bacterial strains: *Escherichia coli* CECT 515 and *Staphylococcus aureus* CECT 240 following the international standard ISO 20776–1:2006. Inoculum solutions were adjusted to a concentration of 10^7 CFU/mL, while the biocide solutions were prepared at concentrations ranging from 0.25 to 1024 mg/L for both types of nanoparticles. The assay was conducted in 96-well plates, where each well contained 100 μL of the biocide, 100 μL of Mueller-Hinton broth at double concentration, and 5 μL of the biocide. Following 24 h of incubation with at 37 °C, the increase in turbidity at 630 nm was measured using an Ultra Microplate reader (BIO-TECK Instruments, model epoch 2). Minimum inhibitory

concentration (MIC) and minimum bactericidal concentration (MBC) were conducted in triplicate. Values were determined from the assay results.

2.7. Antimelanogenic activity

2.7.1. Cell culture and treatments

B16F10 mouse melanoma cells ATCC CRL-6475™ were purchased from American Type Culture Collection (Manassas, VA). The cells were cultured and maintained in Dulbecco's modified Eagle's medium (DMEM; Gibco Life Technologies, Carlsbad, CA, USA) supplemented with 10 % FBS, 1 % antibiotics (penicillin and streptomycin) and 2 mM L-glutamine (at 37 °C with 5 % CO_2 atmosphere. (AgNP-(S-PEG2K-CA)) (**1**) and AgNP-(S-PEG2K-CA)(S-G_1-NMe_3Cl) **(2)** were dispersed in water and further diluted with DMEM to achieve the indicated final concentrations (0.1, 0.5, 1, 5, 10 and 20 μg/mL).

2.7.2. Cell viability assay

3-(4,5-cimethylthiazol-2yl)-2,5-diphenyl tetrazolium bromide (MTT) (Thermo Fisher Scientific, Waltham, MA, USA) cell viability assay was assessed to determine the viability of B16F10 cells following treatment. Cells were seeded at 1×10^4 cells/well in 96 well plates. After treatment with 0.1, 1, 5, 10, 20 or 50 μg/mL of AgNPs, cells were incubated at 37 °C for 48h. Cell viability was determined using MTT solution (1 mg/mL, 50 μL per well), which was added to each well. The cells were then incubated at 37 °C for 4 h. After the removal of the MTT solution, 100 μl Dimethyl sulfoxide (DMSO) was added to the well and incubated for 10min. Absorbance was determined at 595 nm using a microtiter plate reader. To verify that AgNPs did not interfere with the MTT assay, a cell-free control was performed in triplicate under identical experimental conditions but in the absence of cells. The mean absorbance values for AgNPs ranged from 0.133 ± 0.003 to 0.139 ± 0.003, compared to 142 ± 0.007 in the control, indicating no significant difference and confirming the absence of interference with the MTT reagent.

2.7.3. Melanin assay

Cells were cultured at $8x10^4$ cells/ml in 12-well plates and treated with 100 nM of alpha-melanocyte stimulating hormone (α-MSH, Sigma-Aldrich, St. Louis, MO, USA), except for the negative control group. AgNPs were administered at 0.1, 1, 5, 10 or 20 μg/mL for 48 h. For the melanin secretion assay, absorbance of culture media was measured using an optical density reader at 490 nm. Cells from each well were lysed with 300 μL of lysis buffer and pelleted by centrifugation (12,000 rpm, 10 min). The resulting pellets were dissolved in 300 μL buffer (1 M NaOH, 10 % dimethyl sulfoxide (DMSO)) and melted at 80 °C for 30 min. Absorbance was measured at 405 nm using an optical density reader. Experiments were performed in triplicate. To ensure consistency across samples, melanin content was normalized to protein concentrations determined by the BCA Protein Assay Kit (Pierce Biotechnology).

2.7.4. Western blotting

After treatment, B16F10 cells were lysed with RIPA buffer containing protease inhibitor cocktail. A total of 25 μg of protein was loaded and separated by 10 % SDS–PAGE, followed by transfer onto a polyvinylidene difluoride (PVDF) membrane (Millipore). Membranes were blocked with 5 % non-fat milk for 1 h and then were incubated with anti-tyrosinase antibody (Ab 170905, Microphthalmia Transcription Factor (MITF) (Cell Signaling Technology, Danvers, MA, USA 12590)) or anti-beta actin (Sigma-Aldrich, St. Louis, MO, USA A2228) overnight at 4 °C. After washing in PBST, membranes were incubated for 1h with goat anti-rabbit or anti-mouse secondary antibodies. Protein bands were visualized using ECL Western blotting reagents (Pierce), and densitometric analysis were performed using Image J software.

2.7.5. Statistical analysis

One-way ANOVA followed by Dunnett's post hoc test was used to assess statistical significance, comparing each treatment group with the α-MSH-stimulated positive control (set as 100 %). Statistical analysis was performed using GraphPad Prism 5 software (GraphPad Software, La Jolla, CA, USA). A p-value <0.05 was considered statistically significant.

2.8. In vitro permeability study

The *in vitro* skin silver nanoparticles permeation was carried out using Franz diffusion cell system (Vertical Diffusion Cell Test System HDT 1000). This cell consists of two main compartments, the donor and receptor, separated by a Transdermal Diffusion Test Model (Strat-M membrane). The receptor medium was 12 ml of isotonic phosphate buffer solution at pH 7.4, 35 °C and stirred at 600 rpm. At predetermined time points of 0.5, 1, 1.5, 2, 3, 4, 5, 6 and 24 h, 1 mL of the receptor medium was removed, and an equal volume of the isotonic phosphate buffer solution was immediately replaced. All experiments were conducted in triplicate. Finally, the amount of silver nanoparticles was analyzed at different periods of times by the UV–Vis method. The remaining receptor medium was concentrated, and the silver content was measured using ICP-OES Varian-720-ES 9 instrument.

3. Results and discussion

3.1. Synthesis and characterization of silver nanoparticles AgNPs

In the literature, the prevailing approach to synthesizing polyphenolic metal nanoparticles hinges on the capacity of hydroxyl groups within polyphenols to catalyze the reduction of metal centres. However, thiol-metal interactions play a pivotal role in stabilizing metal nanoparticles, owing to the strong affinity of thiol groups for metal surfaces. Thiol groups are avidly adsorbed onto nanoparticles surface, effectively preventing aggregation and ensuring colloidal stability. In this work, we used a commercial thiol, HS-PEG2K-NH_2·HCl, derivatized with caffeic acid previously synthesized in our laboratory [31]. This ligand comprises a polyethylene glycol (PEG) chain, which, owing to its pronounced hydrophilicity, facilitates the facile dispersion of PEG-coated nanoparticles in aqueous environments. This property minimizes friction with biological surfaces, thus mitigating the risk of opsonization and immune recognition [40,41]. By addressing both microbial proliferation and hyperpigmentation properties, a first-generation carbosilane dendron (HS-G_1NMe_3Cl) with ammonium groups on the surface was also anchored to the surface of the AgNP. This dendritic architecture not only amplifies the nanoparticle surface area for interaction with biological membranes but also facilitates precise molecular tuning, ensuring optimal antibacterial efficacy. The presence of ammonium groups further accentuates the bactericidal activity, while the PEG-caffeic ligand concurrently offers depigmenting properties.

In an aqueous medium, the silver precursor ($AgNO_3$) was reduced by $NaBH_4$ in the presence of stabilizing ligand I to synthesize homofunctionalized nanoparticles. Dialysis (MWCO 20 kDa) afforded homofunctionalized AgNP-(S-PEG2K-CA) (**AgNP-1**) as a brown solid dispersed in water. Heterofunctionalized nanoparticles were then readily synthesized in water via the direct reaction of $AgNO_3$ with a mixture of thiol derivatives (**I**, **II**) and $NaBH_4$. These nanoparticles AgNP-(S-PEG2K-CA)(S-G_1NMe_3Cl) (**AgNP-2**) were purified and obtained as a brown solid dispersed in water. (Scheme 1).

The particle size of the AgNPs was studied by Dynamic Light Scattering (DLS) and Transmission Electron Microscopy (TEM) (see Fig S1 and Fig S2). The discrepancy in measurements obtained through both techniques stems arose from differences in their operating principles. TEM provides direct images of individual particles, enabling detailed visualization of particle morphology and size distribution within the sample. TEM images demonstrate the formation of the homo- (**1**) and

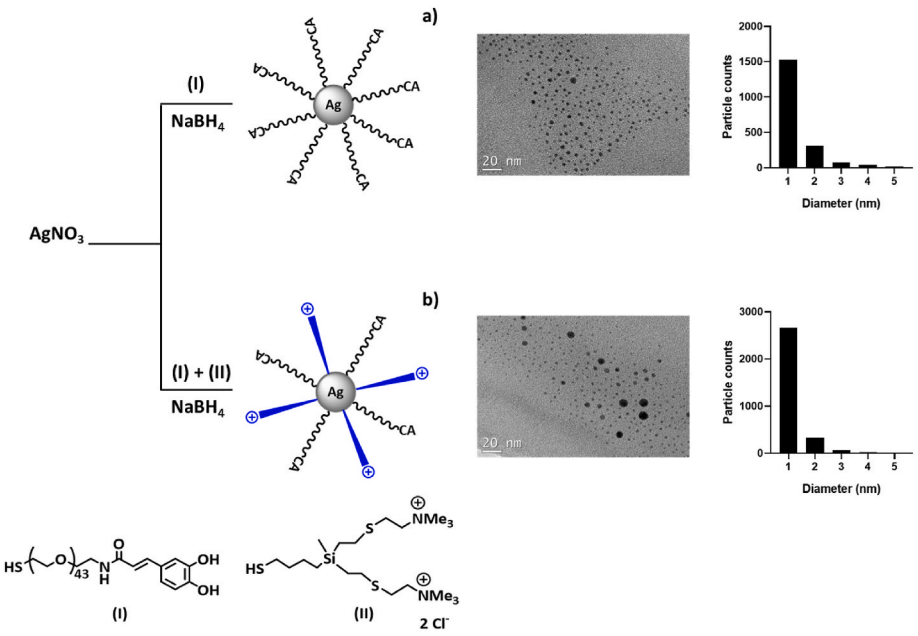

Scheme 1. Synthesis, TEM image and size distribution histogram of **(a)** AgNP-(S-PEG2K-CA) (**AgNP-1**) and **(b)** AgNP-(S-PEG2K-CA)(S-G_1NMe_3Cl) (**AgNP-2**).

hetero-functionalized (**2**) AgNPs. The results underscore that the size and spherical shape of AgNPs remains unaltered regardless of the presence of one or two capping ligands, with the majority of nanoparticles measuring approximately 1 nm in diameter.

On the other hand, DLS furnishes information regarding particle size distribution in solution, encompassing average hydrodynamic size and polydispersity, albeit lacking the capability to reveal specific morphological details and the colloidal stability of the nanoparticles in solution. In this study, the hydrodynamic diameter of the nanoparticles was assessed using volume-weighted distributions obtained from dynamic light scattering (DLS) measurements. For DLS, measurements involve analysing fluctuations in scattered light intensity resulting from the Brownian motion of particles dispersed in a liquid. The Stokes–Einstein equation was applied in this analysis to determine diffusion coefficients and particle hydrodynamic size. The theoretical core diameter of the AgNPs was calculated using the polydispersity value (PDI) of DLS ($\boldsymbol{D_x}/(\mathbf{1}+\boldsymbol{PDI})^5$).

The data presented in Table 1 reveal a larger particle size for the hetero-functionalized nanoparticles **AgNP-2** 24.07 ± 1.69 (hydrodynamic diameter, nm) compared to the homo-functionalized ones **AgNP-1** 18.41 ± 5.50 (hydrodynamic diameter, nm), suggesting that the type of surface functionalization influences the overall particle size. The discrepancy between the particle sizes determined by TEM and DLS, specifically, the larger diameters obtained from DLS measurements, could be attributed to the different principles underlying each technique. In TEM imaging, the measured size corresponds to the projected area of the metallic core, essentially providing a "shadow" of the nanoparticle under vacuum conditions. In contrast, DLS evaluates the hydrodynamic diameter of particles dispersed in solution, which includes not only the metallic core but also contributions from the solvation layer, possible nanoparticle associations or aggregation, and the electrical double layer that develops at the boundary between the nanoparticle surface and the adjacent solvent. The dimension of this electrical double layer, and consequently the hydrodynamic radius, may vary depending on the nanoparticle's surface chemistry and the ionic strength of the dispersion medium. In this work, AgNPs were modified with polyethylene glycol with an average molecular weight of 2000 (PEG2000). To take into account its relatively short chain length, it would be expected to cause only a minor increase in particle size. Nevertheless, when covalently attached to the nanoparticle surface, PEG chains can enlarge the hydrodynamic diameter by several nanometers, depending on their degree of hydration, surface coverage, and conformational flexibility in aqueous media. In addition, the presence of exposed positive charges on the metal surface in **AgNP-2** could promote the formation of aggregates, leading to an increase in size as detected by DLS. This observation aligns with findings from previous studies on other metal nanoparticles [31,42]. The presence of a positive charge on the surface also influences the zeta potential values resulting in more positive values for the nanoparticles containing the carbosilane dendron with peripheral ammonium groups anchored to the metal surface, hetero-functionalized nanoparticles **AgNP-2** (+16.9 ± 3.27 mV), than homo-functionalized **AgNP-1** (+1.80 ± 3.12 mV). From a biological perspective, previous studies have demonstrated the importance of nanoparticle size in determining cellular interactions and biocompatibility. Particles smaller than 20 nm tend to exhibit higher reactivity and cytotoxicity, while those in the 20–50 nm range show efficient receptor-mediated internalization with reduced toxicity [43] Similarly, nanoparticles sized between 10 and 50 nm achieve a balance of colloidal stability, biocompatibility, and effective cellular uptake. In this context, the hydrodynamic diameter observed in our study, 18–24 nm, suggested that the nanoparticles are well-capped and effectively dispersed, remaining within the optimal size range for efficient cellular internalization while minimizing cytotoxicity.

Thermogravimetric analysis (TGA) was conducted to quantify the amount of organic material surrounding the metallic cores. For this purpose, **AgNP-1**, **AgNP-2**, and the capping ligands HS-PEG2K-CA (**I**) and HS-G_1NMe_3Cl (**II**), were heated from 25 to 1000 °C under a nitrogen atmosphere.

The weight loss observed upon heating is attributed to the degradation of organic matter present in the nanoparticles (Fig. 1). Due to the

Table 1
TEM and DLS characterization data of AgNPs.[a] Diameter obtained by TEM, corresponds with the mode value.[b] Polydispersity Index (PDI) in DLS measurements. [c]Hydrodynamic diameter (nm) obtained by DLS. [d]Calculated diameter. [e]Zeta Potential (mV).

	D[a]	PDI[b]	D_x^c	CD_x^d	ZP[e]
AgNP-1	1	0.248	18.41 ± 5.50	6.08	+1.80 ± 3.12
AgNP-2	1	0.265	24.07 ± 1.69	7.43	+16.9 ± 3.27

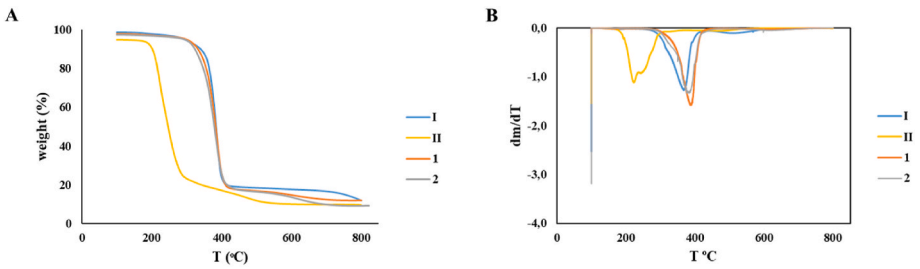

Fig. 1. Graphics of A) weight loss in function of temperature and B) first derivative of the weight loss for capping ligands (HS-PEG2K-CA (**I**) and HS-G_1NMe_3Cl (**II**)), **AgNP-1** and **AgNP-2**.

difference in degradation temperature found in both ligands, 200–300 °C for HS-G_1NMe_3Cl (**II**) and 300–600 °C for HS-PEG2K-CA (**I**), the analysis of the derivative of weight loss with respect to temperature allows quantification of the percentage of each component in the nanoparticles. Significantly, both **AgNP-1** and **AgNP-2** underwent weight loss between 300 and 600 °C, reflecting the decomposition of the S-PEG2K-CA ligands. However, weight loss between 100 and 300 °C, linked to the thermal decomposition of carbosilane dendron S-G_1NMe_3Cl, was observed exclusively in the case of hetero-functionalized **AgNP-2**.

The number of ligands anchored to each AgNP was estimated from the experimental results. Based on the average nanoparticle core diameter determined by TEM (1.0 nm), the number of silver atoms (NAg) of **AgNP-1** and **AgNP-2** was calculated. This estimation assumes spherical nanoparticle shapes and incorporates the weight loss determined by TGA and the determination of AgNPs core area; thus, the average surface coverage (Γ) could be estimated (see Table 2) (see Supplementary Information for details S2).

3.2. Antioxidant activity: chemical-based assays

Polyphenols are widely recognized for their robust antioxidant properties, owing to their capacity to effectively neutralize free radicals and other oxidizing agents within the human body. Considering that free radicals and other reactive oxygen species (ROS) can incite oxidative stress in the skin, thereby fostering irregular pigmentation and other manifestations of cutaneous aging, the antioxidant potential of synthesized nanoparticles has been systematically assessed. Two different chemical-based assays, scavenging activity toward a stable free radical (2,2-diphenyl-1-picrylhydrazyl (DPPH)) and the reduction of metal ions (ferric ion reducing antioxidant potential (FRAP)), were used to determine the antioxidant activity of both **AgNP-1** and **AgNP-2**. The analysis of the results (see Figs. S3 and S4), depicted in Fig. 2, was approached from two distinct perspectives. This involved assessing the IC_{50} (the concentration of antioxidant compound required to scavenge 50 % of DPPH free radicals) and the EC_{50} (the concentration of antioxidant compound needed to enhance the FRAP capacity by 50 %).

Analysis of the data from the DPPH assay revealed that compound **I** had an IC_{50} value of 1.61 μg/mL, indicating outstanding radical-scavenging activity that even surpassed that of free caffeic acid. As expected, **AgNP-1**, which incorporates only derivative **I** in its composition, showed higher activity (IC_{50} = 4.18 μg/mL) than **AgNP-2** (IC_{50} = 12.35 μg/mL), which contains the cationic carbosilane dendritic wedge and ligand **I**.

Table 2
Estimation of [a] the ligands anchored to each AgNPs and[b] total surface coverage based on TGA analysis (% of organic matter) and TEM (1.0 nm AgNP size).

AgNPs	molecule	% TGA	L/AuNP[a]	Γ (Å^2/molecule)[b]
1	-S-PEG2K-CA	88	10	31
2	-S-PEG2K-CA	72	5	45
	-S-G_1-NMe_3Cl	7	2	

The FRAP assay (which measures the ability to reduce iron(III) to iron(II) via a one-electron transfer process) confirmed that the **AgNP-2** was again the least active (EC_{50} = 0.87 μg/mL). Nevertheless, **AgNP-1** (EC_{50} = 0.57 μg/mL) exhibited slightly lower activity than both derivative **I** (EC50 = 0.18 μg/mL) and free caffeic acid (EC50 = 0.21 μg/mL). The results obtained are consistent with what was expected, since nanoparticles exhibited higher EC_{50} values due to their considerable size, which introduces pronounced steric hindrance and limits effective interaction with the Fe^{3+}–TPTZ complex, thereby reducing electron-transfer efficiency.

Overall, the results obtained from both assays demonstrate that the nanoparticles preserve the antioxidant properties of caffeic acid when it is immobilized on their surface. The decrease in activity compared to free caffeic acid may be attributed to structural and conformational factors at the nanoparticle surface. In particular, the flexibility of the PEGylated chains can induce a "back-folding" effect, which may partially shield or reduce the accessibility of caffeic acid units to reactive species, modify the ligand's redox potential and hydrogen-bonding environment. thus leading to a lower apparent antioxidant capacity. In addition, in the case of the heterofunctionalized nanoparticle, the presence of the dendritic wedge reduces the number of caffeic acid units on the surface, further decreasing the overall antioxidant capacity.

3.3. Antibacterial activity

The antibacterial activity of **AgNP-1** and **AgNP-2**, as well as ligands **I** and **II**, was evaluated using *S. aureus* and *E. coli* as models of Gram-positive and Gram-negative bacteria, respectively. The antibacterial activity of silver nanoparticles is generally attributed to the release of silver ions (Ag^+), which can disrupt the bacterial cell membrane, inhibit essential proteins by binding to thiol (-SH) groups, and damage DNA [37].

Table 3 shows the minimum concentrations required for growth inhibition (MIC) and bactericidal activity (MBC) values, respectively. The results indicate that neither the homofunctionalized **AgNP-1** nor the HS-PEG2K-CA (**I**) ligand exhibited antibacterial activity against either strain. In contrast, the heterofunctionalized **AgNP-2** and the dendron demonstrated identical antibacterial effects, with MIC values of 4 mgL^{-1} and MBC of 8 mgL^{-1} against *S. aureus*. This suggests that the antimicrobial activity is primarily attributed to the cationic dendrons. In *E. coli*, the MIC of the **AgNP-2** improved compared to the dendron (**II**), suggesting a modest cooperative effect between the carbosilane dendrons and the silver core. This interpretation is further supported by our previous studies with analogous gold nanoparticles, in which the AuNPs exhibited lower antibacterial activity, demonstrating that replacing gold with silver substantially enhances the antibacterial performance [31].

3.4. Antimelanogenic effect of AgNPs

Melanogenesis is the biosynthetic pathway that produces melanin, with tyrosinase playing a key role by catalyzing its initial and rate-limiting step. Due to its central role in pigmentation, tyrosinase is a

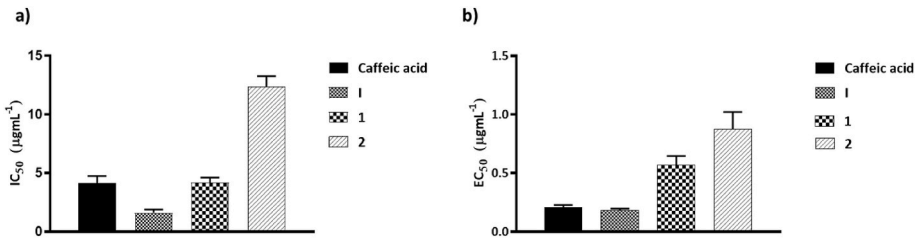

Fig. 2. Antioxidant activity of compounds: IC_{50} in DPPH assay(a), EC_{50} in FRAP assay (b) for caffeic acid HS-PEG2K-CA (I) **AgNP-1** and **AgNP-2**.

Table 3
Values of Minimum inhibitory concentration (MIC) and minimum bactericidal concentration (MBC) are in ppm (mgL^{-1}).

	Staphylococcus aureus		*Escherichia coli*	
Compound	MIC [mg/L]	MBC [mg/L]	MIC [mg/L]	MBC [mg/L]
I	>1024	>1024	>1024	>1024
II	4	8	16	16
AgNP-1	>1024	>1024	>1024	>1024
AgNP-2	4	8	8	16

major target in the development of anti-melanogenic therapies. In this study, the intracellular and extracellular antimelanogenic potential of the new AgNPs were evaluated on B16F10 mouse melanocytes.

As illustrated in Fig. 3a, treatment with **AgNP-1** did not produce a significant reduction in cell viability at any of the concentrations tested. However, treatment with **AgNP-2** led to a decrease in cell viability of 20–25 % decrease in cell viability at higher concentrations (10 and 20 μg/mL), and a 46 % reduction at the highest concentration tested (50 μg/mL), which was not included in the subsequent experiments. The favorable cytotoxicity profile observed for our PEG-coated silver nanoparticles is closely related to their surface chemistry. PEG chains provide a steric barrier that limits direct interactions between silver atoms and cellular components, reducing intrinsic cytotoxicity. However, heterofunctionalization introduces positively charged groups on the nanoparticle surface, which can increase toxicity by destabilizing cellular membranes. Thus, the overall cytotoxicity reflects a balance between the protective effect of PEG and the membrane-disrupting influence of surface-positive charges, highlighting the importance of careful surface engineering to achieve biocompatible yet functional silver nanoparticles.

Regarding antimelanogenic effect of AgNPs, results of melanin content assays are shown in Fig. 3(b–e). For both compounds, concentrations starting at 5 μg/mL significantly reduced extracellular melanin levels compared to the positive control (cells stimulated with α-MSH but untreated). For **AgNP-1**, treatments with doses ≥1 μg/ml reduced extracellular to levels comparable to those of the negative control (unstimulated with α-MSH), and at the highest doses (10 and 20 μg/ml), the effect was even greater than that of kojic acid, well-known depigmenting agent and tyrosinase inhibitor, despite being used at 50-fold lower concentrations. Both compounds at 20 μg/mL also reduced the accumulation of intracellular melanin in a similar extent as kojic acid at 1000 μg/mL. Immunoblot results (Figures f and g) revealed a significant reduction in tyrosinase protein levels after treatment with **AgNP-1** at concentrations of 5, 10, and 20 μg/mL. In contrast, the compound **AgNP-2** only produced a significant reduction in tyrosinase expression at 20 μg/mL, indicating a lower potency in modulating tyrosinase protein levels. Importantly, the ligands alone did not induce any significant change in tyrosinase expression, suggesting that its activity is dependent on nanoparticle conjugation.

Our results reveal a potent anti-melanogenic effect of silver nanoparticles functionalized with caffeic acid **AgNP-1** in B16F10 melanocytes. These nanoparticles significantly reduced both extracellular and intracellular melanin content in a dose-dependent manner and effectively suppressed tyrosinase protein expression. Notably, their inhibitory effect was stronger than that of kojic acid, even when used at concentrations 50 times lower. Moreover, the conjugated nanoparticle clearly improved the activity of free caffeic acid, highlighting the added value of the functionalization strategy. In addition, these results are in agreement with previously reported findings, in which caffeic acid–peptide conjugates employing short linker moieties demonstrated enhanced stability and cellular delivery, leading to a significant suppression of melanin synthesis and downregulation of melanogenesis-associated genes, including *TYR*, *TYRP1*, *TYRP2*, and *MITF*, in SK-MEL-2 melanoma cells [44]. Consistent with these observations, the present study demonstrates that anchoring caffeic acid to nanoparticles similarly enhances its anti-melanogenic efficacy. This finding supports the potential of nanocarrier systems as a promising strategy to improve both the pharmacological activity and cellular bioavailability of melanogenesis-inhibiting agents. To further investigate the molecular basis of the observed inhibition of melanogenesis, the expression of MITF was analyzed under the same experimental conditions (Fig. S6). Although our data were obtained 48 h after α-MSH stimulation and therefore do not capture early events, previous studies have reported that α-MSH transiently induces MITF expression, which subsequently decreases due to feedback down-regulation in melanocytes exposed to prolonged α-MSH stimulation [45]. Interestingly, treatment with both kojic acid and our nanoparticles markedly reduced tyrosinase expression while increasing MITF levels relative to the α-MSH-stimulated control. This apparent divergence likely reflects a compensatory transcriptional response following tyrosinase inhibition rather than activation of melanogenic signaling. Kojic acid reduces tyrosinase stability by chelating the active-site copper ions [46], and the similar pattern observed for our nanoparticles supports the hypothesis that their main effect occurs post-translationally through modulation of tyrosinase stability and maturation. In line with this, caffeic acid has also been reported to chelate transition metal ions, including copper, which further supports the plausibility of this mechanism [45,46]. In our study, free caffeic acid did not inhibit melanogenesis in the cellular model, indicating that conjugation to the nanoparticle surface is required to enhance its stability and enable efficient interaction with tyrosinase. Accordingly, the superior efficacy of **AgNP-1** compared with the heterofunctionalized **AgNP-2** can be attributed to its higher surface density and accessibility of caffeic acid groups, which maximize the number of available catechol sites capable of interacting with tyrosinase. In contrast, the presence of a secondary ligand in compound **2** likely introduces steric hindrance and reduces the effective exposure of active phenolic groups, thereby limiting copper chelation and diminishing overall inhibitory activity.

3.5. *In vitro permeability study*

The evaluation of the ability of synthesized nanoparticles to penetrate the dermal layers is a critical parameter in assessing their potential application as cosmetic agents. This property has been systematically investigated using Franz cell diffusion assays [47]. The Franz diffusion cell assay is a standardized *in vitro* method used to evaluate the permeation of compounds across biological or synthetic membranes that mimic the skin's barrier properties. In this setup, the tested compound is

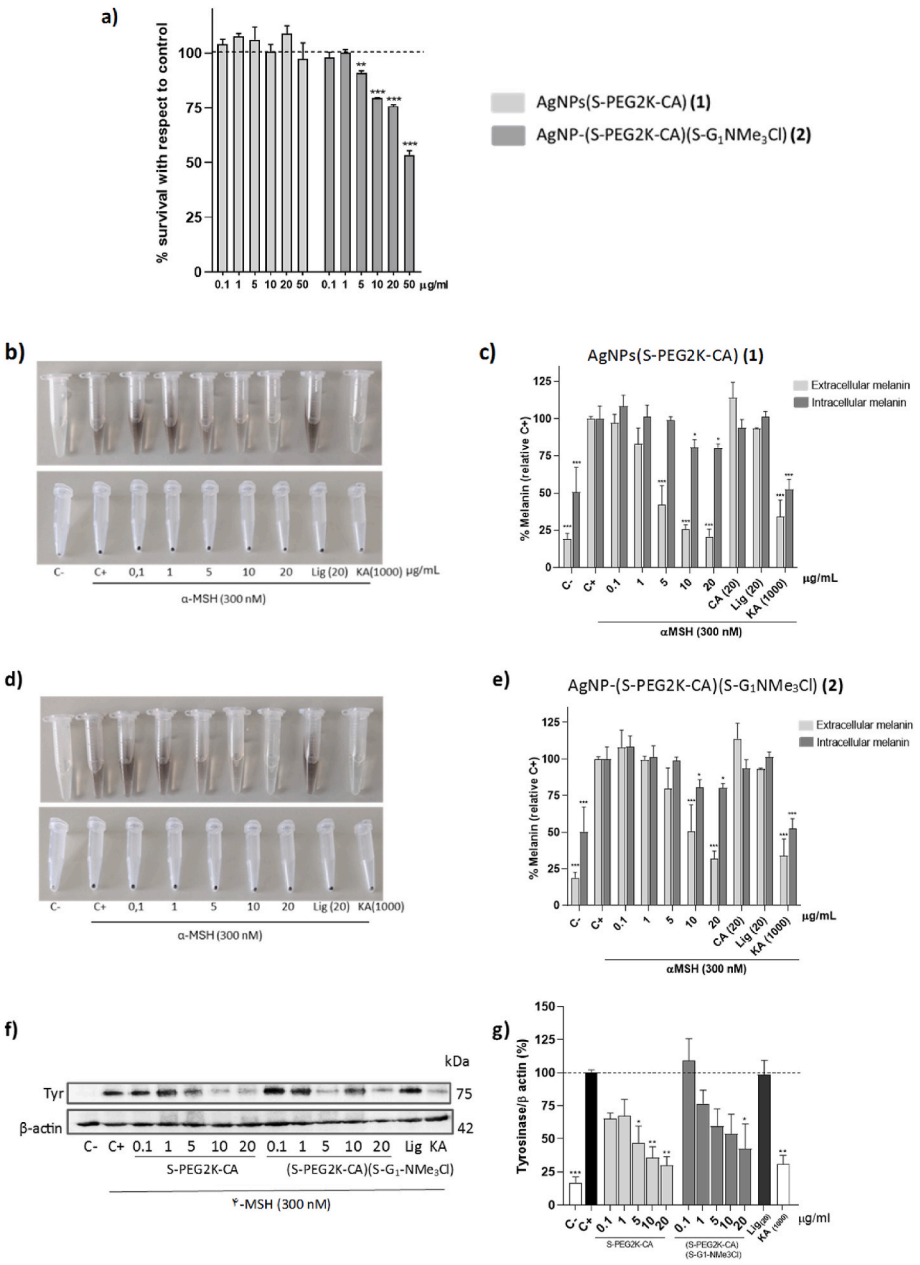

Fig. 3. Cytotoxicity and anti-melanogenic effects of AgNPs in B16F10 melanocytes. Cell viability assessed by MTT assay after treatment with increasing concentrations of AgNPs **(a)**. Appearance of culture media (top), cell pellets (bottom), and melanin content quantification after **AgNP-1 (b, c)** or **AgNP-2 (d, e)** treatments. Representative immunoblot of tyrosinase expression in B16F10 cells treated with AgNPs **(f)** and densitometric analysis **(g)**. Percentage values in the treated cells were compared with respect to that in the untreated control (100 %). CA caffeic acid; Lig: ligand; KA: kojic acid. Data are expressed as mean ± SD for triplicate. *p < 0.05 vs positive control; **p < 0.01 vs positive control; ***p < 0.001 vs positive.

applied to the donor compartment, which represents the skin surface, while the receptor compartment contains a physiological solution maintained at controlled temperature and stirring conditions to simulate dermal microcirculation. The Strat-M® membrane placed between both compartments is a synthetic, non-animal model specifically designed to mimic the barrier properties of human skin. By monitoring the concentration of the compound in the receptor solution over time, the assay provides quantitative information on its ability to penetrate or traverse the Strat-M® membrane.

In this study, we evaluated the ability of both homo- and hetero-functionalized nanoparticles **AgNP-1** and **AgNP-2** to permeate the membrane. The amount of nanoparticle able to cross the membrane was quantified at different time points, from 30 min to 6 h, with samples collected to receptor every hour, and additionally at a longer time point of 24 h. The determination of presence or amount of nanoparticle was carried out using UV–Vis spectroscopy, AgNPs exhibit a characteristic absorption band in the range of 350–450 nm, and ICP-OES. Both analytical techniques yielded consistent results. No UV absorption signals corresponding to AgNPs were detected at any of the measured time intervals, indicating an absence of nanoparticle permeation through the membrane and ICP-OES results showed silver levels below the detection limit, even at parts-per-billion (ppb) sensitivity, indicating that no nanoparticles permeated the membrane under the tested conditions (see Fig. S8). In conclusion, the results demonstrate that neither nanoparticles were able to cross the membrane, indicating that remains confined to the membrane surface which corresponds to the upper layers of the skin. This localization is critical for ensuring a targeted, localized effect while minimizing the risk of systemic exposure, supporting the

safety and suitability of these nanoparticles for topical applications.

4. Conclusions

In summary, this study presents the covalent functionalization of silver nanoparticles (AgNPs) with caffeic acid and the evaluation of their antioxidant, antibacterial, and anti-melanogenic activities in a mammalian melanocyte model. The covalent anchoring of caffeic acid preserves its antioxidant activity, while the heterofunctionalization with a carbosilane wedge imparts antibacterial properties. The integration of these complementary bioactivities into a single nanoscale system enhances, stability and biological efficacy, leading to more pronounced inhibition of melanin synthesis compared to caffeic acid alone. Taken together, these findings support the potential of silver–polyphenol nanoconjugates as promising candidates for cosmetic or therapeutic applications aimed at managing hyperpigmentation. Future studies should focus on evaluating their safety in skin models and confirming their efficacy *in vivo*.

CRediT authorship contribution statement

Siham Bouaouz: Writing – review & editing, Investigation, Formal analysis, Data curation. **Rebeca Lozano:** Investigation, Formal analysis. **Francisca I. Bravo:** Writing – review & editing, Supervision, Conceptualization. **Begoña Muguerza:** Writing – review & editing, Supervision, Resources, Funding acquisition, Conceptualization. **Miquel Mulero:** Writing – review & editing, Supervision, Data curation, Conceptualization. **Enrique Calvo:** Writing – review & editing, Writing – original draft, Supervision, Investigation, Funding acquisition, Formal analysis, Data curation. **Paula Ortega:** Writing – review & editing, Writing – original draft, Supervision, Resources, Methodology, Funding acquisition, Data curation, Conceptualization. **F. Javier de la Mata:** Writing – review & editing, Supervision, Resources, Methodology, Funding acquisition, Conceptualization.

Disclosure of funding

This research was funded by Junta de Comunidades de Castilla la Mancha (SBPLY/23/180225/000109), Instituto de Salud Carlos III through the project FORT23/00046. Comunidad Autónoma de Madrid and European funding from FEDER program (CAM_Radioprotect_P2022BMD-7406) and grant EPU-INV-UAH/2021/002. CIBER-BBN is an initiative funded by the VI National R&D&i Plan 2008–2011, Iniciativa Ingenio 2010, Consolider Program, CIBER Actions, and financed by the Instituto de Salud Carlos III with assistance from the European Regional Development This study was also supported by grants Research to Business from the Universitat Rovira i Virgili (R2B2023/06 and R2B2024/07).

Declaration of competing interest

The authors declare that they have no competing financial or personal interests.

Appendix A. Supplementary data

Supplementary data to this article can be found online at https://doi.org/10.1016/j.jddst.2025.107937.

Data availability

Data will be made available on request.

References

[1] S.A.N. D'Mello, G.J. Finlay, B.C. Baguley, M.E. Askarian-Amiri, Signaling pathways in melanogenesis, Int. J. Mol. Sci. 17 (2016) 1144, https://doi.org/10.3390/ijms17071144.
[2] S. Zolghadri, M. Beygi, T.F. Mohammad, M. Alijanianzadeh, T. Pillaiyar, P. Garcia-Molina, F. Garcia-Canovas, J. Munoz-Munoz, A.A. Saboury, Targeting tyrosinase in hyperpigmentation: current status, limitations and future promises, Biochem. Pharmacol. 212 (2023) 115574, https://doi.org/10.1016/j.bcp.2023.115574.
[3] M.A. Baber, C.M. Crist, N.L. Devolve, J.D. Patrone, Tyrosinase inhibitors: a perspective, Molecules 28 (2023) 5762, https://doi.org/10.3390/molecules28155762.
[4] T. Pillaiyar, V. Namasivayam, M. Manickam, S.-H. Jung, Inhibitors of melanogenesis: an updated review, J. Med. Chem. 61 (2018) 7395–7418, https://doi.org/10.1021/acs.jmedchem.7b00967.
[5] P. Sextius, E. Warrick, A. Prévot-Guéguiniat, G. Lereaux, F. Boirre, L. Baux, S. Ben Hassine, J. Qiu, X.M. Huang, J.Z. Xu, S. Grégoire, S. Ito, K. Wakamatsu, X. Marat, 2-Mercaptonicotinoyl glycine, a new potent melanogenesis inhibitor, exhibits a unique mode of action while preserving melanocyte integrity, Pigment Cell Melanoma Res. 37 (2024) 462–479, https://doi.org/10.1111/pcmr.13168.
[6] J.P. Germanas, E. Unni, K. Kim, T.Y. Germanas, Toward new depigmenting agents through repurposing existing drugs: substituted hydroxyquinolines as melanogenesis inhibitors, J. Invest. Dermatol. 143 (2023) 176–179, https://doi.org/10.1016/j.jid.2022.06.026.
[7] H.-H.K. Lean-Teik Ng, Tzy-Ming Lu potential antioxidants and tyrosinase inhibitors from synthetic polyphenolic deoxybenzoins, Bioorg. Med. Chem. 17 (2009) 4360–4366, https://doi.org/10.1016/j.bmc.2009.05.019.
[8] T.N. Pham, E.A. Cazier, E. Gormally, P. Lawrence, Valorization of biomass polyphenols as potential tyrosinase inhibitors, Drug Discov. Today 29 (2024) 103843, https://doi.org/10.1016/j.drudis.2023.103843.
[9] L.H.N. Alifah, C. Jatmika, H. Hayun, Exploration of ferulic acid and its derivatives as potent anti-tyrosinase: a systematic review, Egypt. J. Chem. 67 (2024) 257–271, https://doi.org/10.21608/ejchem.2023.229107.8427.
[10] A.A. Bhat, G. Gupta, M. Afzal, R. Thapa, H. Ali, S.M. Alqahtani, W.H. Almalki, I. Kazmi, S.I. Alzarea, S. Saleem, V. Subramaniyan, Polyphenol-loaded nanocarriers for breast cancer therapy: a comprehensive review, BioNanoScience 14 (2024) 4219–4237, https://doi.org/10.1007/s12668-023-01288-7.
[11] C. Li, Z. Wang, H. Lei, D. Zhang, Recent progress in nanotechnology-based drug carriers for resveratrol delivery, Drug Deliv. 30 (2023), https://doi.org/10.1080/10717544.2023.2174206.
[12] L. Yang, D. Liu, L. Liu, X. Jiang, Photodynamic effect of vascular-targeted polyphenol nanoparticles on endothelial cells, Photodiagnosis Photodyn. Ther. 47 (2024) 104096, https://doi.org/10.1016/j.pdpdt.2024.104096, 104096.
[13] M. Colic, S. Kraljevic Pavelic, Z. Persuric, A. Agaj, A. Bulog, K. Pavelic, Enhancing the bioavailability and activity of natural antioxidants with nanobubbles and nanoparticles, Redox Rep. 29 (2024) 2333619, https://doi.org/10.1080/13510002.2024.2333619.
[14] V. Rizzi, J. Gubitosa, P. Fini, S. Nuzzo, A. Agostiano, P. Cosma, Snail slime-based gold nanoparticles: an interesting potential ingredient in cosmetics as an antioxidant, sunscreen, and tyrosinase inhibitor, J. Photochem. Photobiol. B Biol. 224 (2021), https://doi.org/10.1016/j.jphotobiol.2021.112309.
[15] J. Pulit-Prociak, A. Grabowska, J. Chwastowski, T.M. Majka, M. Banach, Safety of the application of nanosilver and nanogold in topical cosmetic preparations, Colloids Surf. B Biointerfaces 183 (2019) 110416, https://doi.org/10.1016/j.colsurfb.2019.110416.
[16] I. de la Calle, M. Menta, M. Klein, F. Seby, Screening of TiO_2 and Au nanoparticles in cosmetics and determination of elemental impurities by multiple techniques (DLS, SP-ICP-MS, ICP-MS and ICP-OES), Talanta 171 (2017) 291–306, https://doi.org/10.1016/j.talanta.2017.05.002.
[17] J. Guo, Y. Ping, H. Ejima, K. Alt, M. Meissner, J.J. Richardson, Y. Yan, K. Peter, D. von Elverfeldt, C.E. Hagemeyer, F. Caruso, Engineering multifunctional capsules through the assembly of metal–phenolic networks, Angew. Chem. Int. Ed. 53 (2014) 5546–5551, https://doi.org/10.1002/anie.201311136.
[18] J. Qin, G. Liang, D. Cheng, Y. Liu, X. Cheng, P. Yang, N. Wu, Y. Zhao, J. Wei, Controllable synthesis of iron-polyphenol colloidal nanoparticles with composition-dependent photothermal performance, J. Colloid Interface Sci. 593 (2021) 172–181, https://doi.org/10.1016/j.jcis.2021.02.082.
[19] L.C.F. de Carvalho, Y.A. de Almeida, E.d.S. Machado, N.M. Rodrigues, I.d. F. Gimenez, Polyphenol-mediated preparation of metal nanoparticles: experimental and theoretical study, Chem. Pap. 78 (2024) 1227–1237, https://doi.org/10.1007/s11696-023-03190-8.
[20] M.A. Malik, M.G. Batterjee, M.R. Kamli, K.A. Alzahrani, E.Y. Danish, A. Nabi, Polyphenol-capped biogenic synthesis of noble metallic silver nanoparticles for antifungal activity against *Candida auris*, J. Fungi 8 (2022), https://doi.org/10.3390/jof8060639.
[21] V. Manickam, G. Mani, R. Muthuvel, H. Pushparaj, J. Jayabalan, S.S. Pandit, S. Elumalai, K. Kaliappan, J.H. Tae, Green fabrication of silver nanoparticles and it's *in vitro anti-bacterial, anti-biofilm, free radical scavenging and mushroom tyrosinase efficacy evaluation*, Inorg. Chem. Commun. 162 (2024), https://doi.org/10.1016/j.inoche.2024.112199.
[22] B.O. Gadgeppa, B.M. Raman, G. Mani, G.P. Sidram, S.S. Pandit, J. Jaybalan, K. Kaliappan, H. Pushparaj, J.H. Tae, Phytogenic synthesis of silver nanoparticles using *Achyranthes japonica* root and its *in vitro* antimicrobial, antioxidant, and mushroom tyrosinase inhibitions, Part. Sci. Technol. 42 (2024) 107–119, https://doi.org/10.1080/02726351.2023.2205349.

[23] R.M.G. da Silva, I.D.N. Pereira, L.C. Zibordi, P.A.P. Rosatto, F.O. Granero, C.C. M. Figueiredo, C.J.L. Constantino, C.d.S. Martin, A.E. Job, N. Nicolau-Junior, L. P. Silva, Cytotoxic, antioxidant, and antiglycation activities, and tyrosinase inhibition using silver nanoparticles synthesized by leaf extract of *Solanum aculeatissimum* Jacq, J. Toxicol. Environ. Health A Curr. Issues 87 (2024) 57–76, https://doi.org/10.1080/15287394.2023.2275691.

[24] A.d.C. Gomes, L.C. Zibordi, F.O. Granero, V.F. Ximenes, N.M. Pavan, L.P. Silva, C.d. S.M. Sonvesso, A.E. Job, N. Nicolau, R.M.G.d. Silva, Biosynthesis of silver nanoparticles of *Tribulus terrestris* food supplement and evaluated antioxidant activity and collagenase, elastase and tyrosinase enzyme inhibition: ***in vitro*** and **in silico** approaches, Food Bioprod. Process. 138 (2023) 150–161, https://doi.org/10.1016/j.fbp.2023.01.010.

[25] M. Vaezi, Structure and inhibition mechanism of some synthetic compounds and phenolic derivatives as tyrosinase inhibitors: review and new insight, J. Biomol. Struct. Dynam. 41 (2023) 4798–4810, https://doi.org/10.1080/07391102.2022.2069157.

[26] I.E. Orhan, F.S.S. Deniz, Inhibition of melanogenesis by some well-known polyphenolics: a review, Curr. Pharm. Biotechnol. 22 (2021) 1412–1423, https://doi.org/10.2174/1386207323666201211102233.

[27] S. Hu, J. Huang, S. Pei, Y. Ouyang, Y. Ding, L. Jiang, J. Lu, L. Kang, L. Huang, H. Xiang, R. Xiao, Q. Zeng, J. Chen, Ganoderma lucidum polysaccharide inhibits UVB-induced melanogenesis by antagonizing cAMP/PKA and ROS/MAPK signaling pathways, J. Cell. Physiol. 234 (2019) 7330–7340, https://doi.org/10.1002/jcp.27492.

[28] H.J. Jung, D.C. Choi, S.G. Noh, H. Choi, I. Choi, I.Y. Ryu, H.Y. Chung, H.R. Moon, New benzimidazothiazolone derivatives as tyrosinase inhibitors with potential anti-melanogenesis and reactive oxygen species scavenging activities, Antioxidants 10 (2021) 1078, https://doi.org/10.3390/antiox10071078.

[29] S.Y. Park, M.L. Jin, Y.H. Kim, Y. Kim, S.-J. Lee, Aromatic-turmerone inhibits α-MSH and IBMX-induced melanogenesis by inactivating CREB and MITF signaling pathways, Arch. Dermatol. Res. 303 (2011) 737–744, https://doi.org/10.1007/s00403-011-1155-7.

[30] C. Magnani, V.L.B. Isaac, M.A. Correa, H.R.N. Salgado, Caffeic acid: a review of its potential use in medications and cosmetics, Anal. Methods 6 (2014) 3203–3210, https://doi.org/10.1039/C3AY41807C.

[31] S. Bouaouz, M. Chavez, C.E. Peña González, D. Rojas, A. Escarpa, P. Ortega, F. Javier de la Mata, Enhancing polyphenol delivery and efficacy using functionalized gold nanoparticles: Antioxidant and antibacterial properties, Bioinorgan. Chem. Appl. 2025 (2025) 3836765, https://doi.org/10.1155/bca/3836765.

[32] N. Sanz Del Olmo, C.E. Peña González, J.D. Rojas, R. Gómez, P. Ortega, A. Escarpa, F.J. de la Mata, Antioxidant and antibacterial properties of carbosilane dendrimers functionalized with polyphenolic moieties, Pharmaceutics 12 (2020), https://doi.org/10.3390/pharmaceutics12080698.

[33] N. Pavlíková, Caffeic acid and diseases-mechanisms of action, Int. J. Mol. Sci. 24 (2022), https://doi.org/10.3390/ijms24010588.

[34] C.M. Spagnol, L.D. Di Filippo, V.L.B. Isaac, M.A. Correa, H.R.N. Salgado, Caffeic acid in dermatological formulations: in vitro release profile and skin absorption, Comb. Chem. High Throughput Screen. 20 (2017) 675–681, https://doi.org/10.2174/1386207320666170602090448.

[35] H. Jo, M. Choi, J. Sim, M. Viji, S. Li, Y.H. Lee, Y. Kim, S.-Y. Seo, Y. Zhou, K. Lee, W.-J. Kim, J.T. Hong, H. Lee, J.-K. Jung, Synthesis and biological evaluation of caffeic acid derivatives as potent inhibitors of α-MSH-stimulated melanogenesis, Bioorg. Med. Chem. Lett 27 (2017) 3374–3377, https://doi.org/10.1016/j.bmcl.2017.06.011.

[36] N. Armstrong, M. Ramamoorthy, D. Lyon, K. Jones, A. Duttaroy, Mechanism of silver nanoparticles action on insect pigmentation reveals intervention of copper homeostasis, PLoS One 8 (2013) e53186, https://doi.org/10.1371/journal.pone.0053186.

[37] A. Barrios-Gumiel, J. Sanchez-Nieves, J. Perez-Serrano, R. Gomez, F. Javier de la Mata, PEGylated AgNP covered with cationic carbosilane dendrons to enhance antibacterial and inhibition of biofilm properties, Int. J. Pharm. 569 (2019) 118591, https://doi.org/10.1016/j.ijpharm.2019.118591.

[38] E. Fuentes-Paniagua, J.M. Hernandez-Ros, J. Soliveri, J.L. Copa-Patino, R. Gomez, J. Sanchez-Nieves, F. Javier de la Mata, Strategies for penicillin V dendronization with cationic carbosilane dendrons and study of antibacterial properties, Can. J. Chem. 95 (2017) 927–934, https://doi.org/10.1139/cjc-2017-0059.

[39] C.E. Peña-González, E. Pedziwiatr-Werbicka, D. Shcharbin, C. Guerrero-Beltrán, V. Abashkin, S. Loznikova, J.L. Jiménez, M.Á. Muñoz-Fernández, M. Bryszewska, R. Gómez, J. Sánchez-Nieves, F.J. de la Mata, Gold nanoparticles stabilized by cationic carbosilane dendrons: synthesis and biological properties, Dalton Trans. 46 (2017) 8736–8745, https://doi.org/10.1039/C6DT03791G.

[40] J.S. Suk, Q. Xu, N. Kim, J. Hanes, L.M. Ensign, PEGylation as a strategy for improving nanoparticle-based drug and gene delivery, Adv. Drug Deliv. Rev. 99 (2016) 28–51, https://doi.org/10.1016/j.addr.2015.09.012.

[41] L. Shi, J. Zhang, M. Zhao, S. Tang, X. Cheng, W. Zhang, W. Li, X. Liu, H. Peng, Q. Wang, Effects of polyethylene glycol on the surface of nanoparticles for targeted drug delivery, Nanoscale 13 (2021) 10748–10764, https://doi.org/10.1039/D1NR02065J.

[42] A. Barrios-Gumiel, J. Sánchez-Nieves, E. Pedziwiatr-Werbicka, V. Abashkin, N. Shcharbina, D. Shcharbin, S. Glińska, K. Ciepluch, D. Kuc-Ciepluch, D. Lach, M. Bryszewska, R. Gómez, F.J. de la Mata, Effect of PEGylation on the biological properties of cationic carbosilane dendronized gold nanoparticles, Int. J. Pharm. 573 (2020) 118867, https://doi.org/10.1016/j.ijpharm.2019.118867.

[43] Q. Xia, J. Huang, Q. Feng, X. Chen, X. Liu, X. Li, T. Zhang, S. Xiao, H. Li, Z. Zhong, K. Xiao, Size- and cell type-dependent cellular uptake, cytotoxicity and in vivo distribution of gold nanoparticles, Int. J. Nanomed. 14 (2019) 6957–6970, https://doi.org/10.2147/ijn.S214008.

[44] K.-Y. Park, J. Kim, Synthesis and biological evaluation of the anti-melanogenesis effect of coumaric and caffeic acid-conjugated peptides in human melanocytes, Front. Pharmacol. 11 (2020), https://doi.org/10.3389/fphar.2020.00922, 2020.

[45] D.H. Lee, S.S. Ahn, J.-B. Kim, Y. Lim, Y.H. Lee, S.Y. Shin, Downregulation of α-Melanocyte-Stimulating hormone-induced activation of the Pax3-MITF-Tyrosinase axis by sorghum ethanolic extract in B16F10 melanoma cells, Int. J. Mol. Sci. 19 (2018) 1640.

[46] R. Cardoso, R. Valente, C.H. Souza da Costa, J.L. da S. Gonçalves Vianez, K. Santana da Costa, F.A. de Molfetta, C. Nahum Alves, Analysis of Kojic acid derivatives as competitive inhibitors of tyrosinase: a molecular modeling approach, Molecules 26 (2021) 2875.

[47] A. Simon, M.I. Amaro, A.M. Healy, L.M. Cabral, V.P. de Sousa, Comparative evaluation of rivastigmine permeation from a transdermal system in the Franz cell using synthetic membranes and pig ear skin with in vivo-in vitro correlation, Int. J. Pharm. 512 (2016) 234–241.